

Optical Monitoring of Quasars: I. Variability

Aurea Garcia^{1*}, Laerte Sodré Jr.^{1†}, Francisco J. Jablonski^{2‡} & Roberto J. Terlevich^{3§}

¹*Departamento de Astronomia, Instituto Astronômico e Geofísico da USP, Av. Miguel Stefano 4200, 04301-904 São Paulo, Brazil*

²*Departamento de Astrofísica INPE/MCT, CP151, 12201 São José dos Campos, Brazil*

³*Institute of Astronomy, Madingley Road, Cambridge CB3 0HA*

11 June 2021

ABSTRACT

We present an analysis of quasar variability from data collected during a photometric monitoring of 50 objects carried out at CNPq/Laboratório Nacional de Astrofísica, Brazil, between March 1993 and July 1996. A distinctive feature of this survey is its photometric accuracy, ~ 0.02 V mag, achieved through differential photometry with CCD detectors, what allows the detection of faint levels of variability. We find that the relative variability, $\delta = \sigma/L$, observed in the V band is anti-correlated with both luminosity and redshift, although we have no means of discovering the dominant relation, given the strong coupling between luminosity and redshift for the objects in our sample. We introduce a model for the dependence of quasar variability on frequency that is consistent with multi-wavelength observations of the nuclear variability of the Seyfert galaxy NGC 4151. We show that correcting the observed variability for this effect slightly increases the significance of the trends of variability with luminosity and redshift. Assuming that variability depends only on the luminosity, we show that the corrected variability is anti-correlated with luminosity and is in good agreement with predictions of a simple Poissonian model. The energy derived for the hypothetical pulses, $\sim 10^{50}$ erg, agrees well with those obtained in other studies. We also find that the radio-loud objects in our sample tend to be more variable than the radio-quiet ones, for all luminosities and redshifts.

Key words: galaxies: active - quasars: general - techniques: photometric - methods: statistical

1 INTRODUCTION

Although variability is a well known property of quasars and Seyfert 1 galaxies, many of its properties are still subject of debate. As noticed by Pica & Smith (1983), studying the dependence of the variability on the luminosity may allow to verify whether the variability is Poissonian or not, that is, whether the source is intrinsically multiple (like compact supernova remnants evolving in a nuclear starburst; e.g., Terlevich et al. 1992) or may be considered as a single co-

herent source (like an accretion disk around a massive black hole; e.g., Rees 1984).

A main prediction of the sub-units model, as sometimes the Poissonian model is called, is that the variability (measured in magnitudes) should be anti-correlated with the source luminosity. Such a behaviour was observed in some early studies (e.g., Uomoto, Wills & Wills 1976; Pica & Smith 1983) and, more recently, in the analysis of the samples SA 94 (Cristiani, Vio & Andreani 1990) and SA 57 (Trevese et al. 1994), as well as in the study of the SGP sample (Hook et al. 1994). These three samples were jointly revisited by Cristiani et al. (1996), that confirmed the anti-correlation obtained previously. However, most of these studies obtained a logarithmic slope for the relation between variability and luminosity shallower than the value -0.5 that is expected in the simple Poissonian model (see section 4.1). The same result was achieved by Paltani & Courvoisier (1997), who analyzed the ultraviolet continuum

* e-mail: aurea@iagusp.usp.br

† e-mail: laerte@iagusp.usp.br

‡ e-mail: chico@das.inpe.br

§ e-mail: rjt@ast.cam.ac.uk; visiting professor at Instituto Nacional de Astrofísica, Óptica y Electrónica, Tonantzintla, Puebla, Mexico

of all Seyfert 1 galaxies, radio-quiet quasars, and low polarization radio-loud quasars contained in the IUE database. However, other studies have indeed shown evidence for a Poissonian behaviour. For instance, Cid Fernandes, Aretxaga & Terlevich (1996) analyzed the variability of the SGP sample with respect to the luminosity and redshift, obtaining a logarithmic slope consistent with the expected value of -0.5. Also, Aretxaga, Cid Fernandes & Terlevich (1997) have shown that the variability of the SGP sample can be well-reproduced by a random superposition of discrete events.

However, even the very existence of an anti-correlation between variability and luminosity has been disputed. For instance, Lloyd (1984), Cimatti, Zamorani & Marano (1993), and Netzer et al. (1996) have found no dependence of variability on absolute magnitude. Such a controversy probably arises from the different characteristics of the samples studied and procedures used to analyze them. Only recently CCDs have been introduced in quasar monitoring campaigns, improving the accuracy of data and allowing the detection of low levels of variability (see, for instance, Borgeest & Schramm 1994, Netzer et al. 1996 and Giveon et al. 1999). Besides, most of the monitored samples present a strong coupling between luminosity and redshift, typical of flux limited samples. Undoubtedly, this is a major problem of the available data sets, because it prevents one of disentangling the real dependence of the variability on these two parameters. In particular, Cristiani et al. (1996) divided their data in slices in luminosity and redshift, and concluded that there was a significant positive correlation of the variability with redshift. This trend had already been detected by Giallongo, Trevese & Vagnetti (1991), and was interpreted as resultant of a variability vs. wavelength dependence (see below). Cid Fernandes, Aretxaga & Terlevich (1996) also supported this hypothesis to explain the positive correlation between variability and redshift found in their fits.

The increase of the variability with increasing frequency has been observed by many authors (e.g., Cutri et al. 1985; Edelson, Krolik & Pike 1990; Kinney et al. 1991; Paltani & Courvoisier 1994; Cristiani et al. 1997; Paltani, Courvoisier & Walter 1998). A good example of such behaviour in a low luminosity AGN can be seen in Edelson et al. (1996), that contains multi-wavelength variability data of NGC 4151, monitored through the AGN Watch consortium. The parameterization of this trend is of serious concern, because observations in a given photometric band sample different parts of the rest-frame spectrum of quasars at different redshifts. Of course, such effect should be taken in to account in the analysis of the variability of large samples of quasars. If well understood, this effect can be used to constrain models for the nature of quasars and other forms of AGN.

In this paper we present the first results of a monitoring of 50 quasars that has been conducted at the CNPq/Laborat rio Nacional de Astrof sica, in Brazil, since 1993. The observations discussed here were done with a 0.6m telescope in the *V* band during the period between March 1993 and July 1996. The observational strategy is based on differential photometry with CCD detectors. This provides good photometric accuracy, necessary to detect very low levels of variability. These observations will be used to address

several issues regarding the optical variability of quasars. In particular, we discuss here the relation of variability with luminosity, including a model for the dependence of variability on frequency. We will also re-examine whether a simple Poissonian model is consistent with the observations, using a robust fitting technique. We will also compare the variability properties of the radio-loud and radio-quiet objects present in our sample. In another paper, we will present an analysis of the structure function of the light-curves, useful to estimate the variability time-scales of quasars (Garcia et al., in preparation).

This paper is organized as follows. Section 2 presents our sample and a description of the observations and data reduction, as well as the light curves of the quasars. In section 3 we present our estimator of quasar variability and a simple model for correcting the observations of the dependence of variability with frequency. In section 4 we present the simple Poissonian model and examine whether it is able to explain our observations, taking into account the correction for the variability vs. frequency effect. In section 5 we compare the variability observed in the radio-loud and radio-quiet subsamples and, finally, we summarize our conclusions in section 6.

2 THE DATA

2.1 The Sample

The sample of 50 quasars discussed here was drawn from table 1 of V ron-Cetty & V ron (1987) catalog. All quasars have redshifts larger than 0.15 and V-band apparent magnitudes brighter than 16.5 mag in the catalog. The former criterion aimed to minimize the light contribution from the host galaxy, whereas the latter ensured that the sample was bright enough to make the measurement errors small, less than 0.05 mag. Classifying objects with radio emission at 5 GHz larger than 10^{25} W Hz⁻¹ as radio-loud (Kellermann et al. 1994), there are 35 radio-loud and 15 radio-quiet quasars in the sample. Among the radio-loud objects, one BL Lac (PKS 0537-441) was accidentally selected, because it appeared in the 1987 version of the V ron-Cetty & V ron catalog as a ‘‘normal’’ quasar, an error corrected in more recent versions of that catalog.

The sample is presented in Table 1. The columns of the table give, for each object, its name, the equatorial coordinates α and δ (J2000), the radio class R (L: radio-loud, Q: radio-quiet), the redshift *z*, the mean apparent and absolute *V* magnitudes (*V* and *M_V*), the number of observed epochs (*n_e*), the observer and rest-frame time coverage (Δt_{obs} , Δt_{rest} , in years), and the observed relative variability ($\delta_{obs} = (\sigma/L)_{obs}$) and the mean relative measurement error ($\delta_\epsilon = \epsilon/L$) in the *V* band. Three objects in the sample are high polarization quasars (see table 1) according to V ron-Cetty & V ron (1993) or NED[¶]; one of them is the blazar PKS 0537-441. The apparent *V* magnitudes in table 1

[¶] The NASA/IPAC Extragalactic Database is operated by the Jet Propulsion Laboratory, California Institute of Technol-

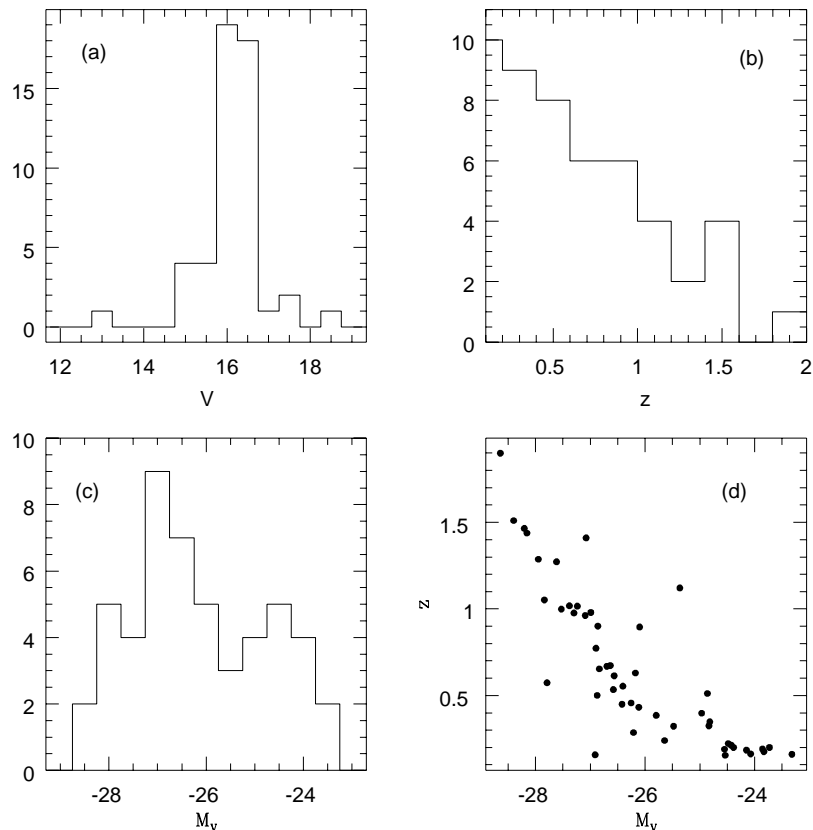


Figure 1. Distribution of the sample in (a) apparent V magnitudes, (b) redshift, and (c) absolute V magnitudes. It is also shown the Hubble diagram of the sample (panel 1-d).

were computed from our photometric calibration for all but 5 quasars (see table 1) for which we adopted magnitudes from Véron-Cetty & Véron (1993; see below).

The absolute magnitudes in table 1 were computed assuming that the optical-UV continuum of quasars may be described by a power-law $f_\nu \propto \nu^\alpha$ with spectral index $\alpha = -0.3$ (Francis 1996, Peterson 1997). Besides the k -correction, we have also included an empirical correction that takes into account the presence of emission lines and the Lyman forest on the measured continuum (Véron-Cetty & Véron 1993). The reddening was corrected from the A_B values given by NED, assuming that $A_V = 0.77 A_B$ (Allen 1976). Luminosity distances were computed assuming $H_0 = 50 \text{ km s}^{-1} \text{ Mpc}^{-1}$, $\Omega_0 = 1$, and $\Lambda = 0$.

Figure 1 shows some features of the sample discussed here. Figure 1-a indicates that most of the objects in the sample have indeed mean apparent magnitudes around $V = 16$ (median $V = 16.17$). The redshift distribution is presented in figure 1-b (median $z = 0.54$). Figure 1-c presents the M_V distribution (median $M_V = -26.4$). The peak

around $M_V \simeq -24.5$ is due to radio-quiet, low redshift objects. The Hubble diagram, i.e., $M_V \times z$, is shown in figure 1-d. Note how strongly luminosity and redshift are correlated in this sample. This happens because, although the quasars in the sample span a large range of redshifts, most of them have mean apparent V magnitudes around 16.

2.2 Observations and Data Reduction

The observations were carried out at the 0.6m Boller & Chivens telescope located at the Observatório do Pico dos Dias, operated by the CNPq/Laboratório Nacional de Astrofísica, in Brazil, during the period from March 1993 to July 1996. We used basically two observational setups: one with the imaging camera coupled directly to a 770×1152 pixels EEV CCD, and the other with a focal reducer plus a 385×578 pixels EEV CCD, in order to have a field of view of about $7' \times 11'$ in both cases. This field is large enough to allow the simultaneous observation of the quasar and some reference stars for the differential photometry. All observations were made in the V band, with two combinations of filters (GG495/2+BG18/2 or GG495+BG39/3, Bessel 1990); we have verified that the differential magnitudes obtained with these two filters are essentially the same. The quasar

ogy, under contract with the National Aeronautics and Space Administration.

Table 1. Description of the sample and observational information.

Quasar	α (2000)	δ (2000)	R ⁽²⁾	z	V	M_V	n_e	Δt_{obs} (yr)	Δt_{rest} (yr)	δ_{obs} (V band)	δ_ϵ (V band)
UM 18	00 05 20.2	+05 24 12	L	1.899	16.29	-28.64	7	2.74	0.95	0.038	0.022
PKS 0003+15	00 05 59.2	+16 09 50	L	0.450	15.62	-26.42	6	2.74	1.89	0.103	0.016
PKS 0005-239	00 07 56.1	-23 41 17	L	1.410	17.32	-27.08	5	2.74	1.138	0.017	0.018
PG 0043+039	00 45 47.2	+04 10 24	Q	0.385	15.89 ⁽³⁾	-25.80	9	2.82	2.03	0.056	0.047
Mark 1014	01 59 50.1	+00 23 43	Q	0.163	15.69 ⁽³⁾	-24.07	6	2.02	1.74	0.084	0.048
3C 57	02 01 57.1	-11 32 32	L	0.669	16.14	-26.70	6	1.95	1.17	0.060	0.017
PKS 0232-04	02 35 07.2	-04 02 05	L	1.438	16.26	-28.16	7	1.94	0.80	0.060	0.019
PKS 0312-77	03 11 55.3	-76 51 51	L	0.223	16.10 ⁽³⁾	-24.48	8	3.40	2.78	0.122	0.049
3C 95	03 51 28.5	-14 29 08	L	0.614	16.11	-26.56	7	1.94	1.20	0.258	0.016
3C 94	03 52 30.5	-07 11 01	L	0.962	16.45	-27.09	7	1.94	0.99	0.023	0.015
PKS 0355-483	03 57 22.0	-48 12 16	L	1.016	16.38 ⁽³⁾	-27.24	8	3.25	1.61	0.027	0.047
PKS 0405-12	04 07 48.3	-12 11 35	L	0.574	14.78	-27.79	7	1.94	1.23	0.074	0.015
3C 110	04 17 16.7	-05 53 45	L	0.773	16.20	-26.90	5	1.94	1.10	0.028	0.016
PKS 0454-22	04 56 08.9	-21 59 09	L	0.534	15.80	-26.58	5	2.18	1.42	0.106	0.017
PKS 0537-441 ⁽¹⁾	05 38 50.3	-44 05 09	L	0.896	16.48 ⁽³⁾	-26.10	8	3.32	1.75	1.483	0.124
PKS 0637-75	06 35 46.5	-75 16 17	L	0.654	16.09	-26.84	9	3.47	2.10	0.188	0.014
PKS 0736+01 ⁽¹⁾	07 39 17.9	+01 37 05	L	0.191	16.31	-23.86	8	2.41	2.02	0.547	0.033
PKS 0743-67	07 43 31.6	-67 26 26	L	1.510	16.34	-28.40	8	3.47	1.38	0.124	0.030
PKS 0837-12	08 39 50.5	-12 14 34	L	0.200	16.52	-23.73	9	2.60	2.16	0.212	0.012
DW 0839+18	08 42 05.0	+18 35 41	L	1.272	16.54	-27.62	9	2.41	1.06	0.153	0.014
PG 0923+201	09 25 54.6	+19 54 05	Q	0.190	15.58	-24.55	10	2.60	2.18	0.093	0.012
PKS 0925-203	09 27 51.7	-20 34 51	L	0.348	16.65	-24.82	10	2.60	1.92	0.100	0.018
PG 1001+05	10 04 20.1	+05 13 01	Q	0.161	16.41	-23.32	10	2.59	2.23	0.066	0.015
PKS 1004+13	10 07 26.1	+12 48 57	L	0.240	14.98	-25.64	10	3.14	2.53	0.144	0.012
PG 1008+133	10 11 10.8	+13 04 13	Q	1.287	16.27	-27.95	7	3.14	1.37	0.027	0.014
PG 1012+00	10 14 54.8	+00 33 37	Q	0.185	15.90	-24.15	8	3.14	2.65	0.074	0.015
PG 1151+117	11 53 49.3	+11 28 31	Q	0.176	16.10	-23.83	9	3.14	2.67	0.084	0.012
3C 273	12 29 06.7	+02 03 09	L	0.158	12.76	-26.91	10	3.14	2.71	0.121	0.016
PG 1254+047	12 56 59.9	+04 27 35	Q	1.018	16.24	-27.38	10	3.14	1.56	0.057	0.010
PKS 1302-102	13 05 32.9	-10 33 20	L	0.286	14.82	-26.21	11	3.22	2.50	0.089	0.217
PG 1307+085	13 09 47.0	+08 19 51	Q	0.155	15.12	-24.54	6	0.41	0.35	0.063	0.173
PG 1333+176	13 36 02.0	+17 25 14	Q	0.554	16.06	-26.41	10	2.09	1.34	0.029	0.117
1E 1352+1820	13 54 35.6	+18 05 19	Q	0.977	16.22	-27.30	5	0.33	0.17	0.011	0.043
PG 1352+011	13 54 59.8	+00 52 50	Q	1.121	18.51	-25.36	8	3.22	1.52	0.066	0.059
PKS 1912-549	19 16 39.2	-54 54 47	L	0.398	16.76	-24.97	17	3.16	2.26	0.187	0.022
PKS 2021-330	20 24 35.5	-32 53 36	L	1.465	16.30	-28.20	16	3.82	1.55	0.066	0.013
PG 2112+059	21 14 52.6	+06 07 44	Q	0.457	15.84	-26.26	14	3.22	2.21	0.035	0.016
PKS 2115-30	21 18 10.5	-30 19 10	L	0.980	16.61	-26.99	10	2.82	1.42	0.089	0.017
PKS 2128-12	21 31 35.2	-12 07 04	L	0.501	15.40	-26.87	10	2.82	1.88	0.068	0.031
PKS 2135-14	21 37 45.1	-14 32 55	L	0.200	15.83	-24.39	9	2.09	1.74	0.237	0.040
OX 169	21 43 35.5	+17 43 49	L	0.213	16.04	-24.43	10	2.67	2.20	0.140	0.032
PKS 2145+06	21 48 05.4	+06 57 40	L	0.999	16.07	-27.53	9	2.67	1.34	0.144	0.023
PKS 2216-03	22 18 52.0	-03 35 36	L	0.901	16.52	-26.86	7	2.09	1.10	0.049	0.068
PG 2233+134	22 36 07.7	+13 43 56	Q	0.325	16.50	-24.84	11	3.22	2.43	0.041	0.056
PKS 2243-123 ⁽¹⁾	22 46 18.2	-12 06 51	L	0.630	16.61	-26.18	9	2.82	1.73	0.106	0.084
PKS 2251+11	22 54 10.4	+11 36 40	L	0.323	15.85	-25.48	8	2.67	2.02	0.050	0.090
PKS 2300-683	23 03 43.6	-68 07 37	L	0.512	17.40	-24.86	10	3.82	2.53	0.120	0.046
PG 2302+029	23 04 44.9	+03 11 47	Q	1.052	15.95	-27.84	8	2.75	1.34	0.053	0.011
4C 09.72	23 11 17.7	+10 08 18	L	0.432	15.82	-26.12	6	2.75	1.92	0.133	0.079
PKS 2344+09	23 46 36.7	+09 30 46	L	0.673	16.28	-26.64	7	2.75	1.64	0.056	0.014

Notes: (1) high polarization quasars; (2) radio class: radio-loud (L) or radio-quiet (Q); (3) objects for which the V magnitudes were taken from V eron-Cetty & V eron (1993).

fields were observed with two successive exposures, each of them of 5 minutes, to minimize cosmic ray contamination. This integration time allow us to achieve a photometric accuracy of a few hundredths of magnitude for most of the objects in the sample.

The data were reduced using IRAF ^{||} standard pack-

^{||} IRAF is distributed by National Optical Astronomy Observatories, which is operated by the Association of Universities for Research in Astronomy, Inc., under contract with the National Science Foundation.

ages for CCD reduction and photometry. The images were first bias and flat-field corrected using the package *ccdred*. The magnitudes were measured from aperture photometry through the *phot* task in the *daophot* package. In each epoch (corresponding to each observational run) we extracted magnitudes within several aperture radii, and then chose the radius which minimized the photometric errors.

Differential photometry is done with respect to reference stars observed in the same field as the quasars. The procedure we devised to select these stars for each field is as follows. First, we selected the brightest isolated stellar sources as possible reference stars for that field. After, we computed magnitude differences between pairs of stars, selecting as reference the star that presented the lowest magnitude dispersion relative to the others during all epochs.

By analyzing multiple observations of several fields, we detected a median underestimation of the photometric errors given by *phot* by a factor of 1.73, similar to that obtained by Gopal-Krishna, Sagar & Wiita (1995), of 1.75. After intensive study of the possible causes of this underestimation, we concluded that it could be originated by random fluctuations of the PSF over the image, probably induced by flat field errors. In fact, large scale fluctuations produced by the dome flat fields used in the reduction may well increase the errors to the observed values. To overcome this problem, we decided to adopt a minimum error of 0.01 mag for each individual magnitude extraction, since this is the expected photometric error of a $V=16$ object with the observational setup used in the observations.

We performed magnitude calibrations by observing standard stars. These observations were done in 7 nights, during runs in March, May, July and August of 1996, and May 1997. The standard stars were selected from Graham (1982) list, and observed for different air masses every two hours during the calibration nights. As the observations were conducted at only one band (V), we have taken into account only the extinction coefficient of first order, associated with the airmass, to determine the apparent magnitudes of the reference star in each quasar field. These observations allowed us to calibrate the magnitudes of 45 quasars. The remaining 5 quasars not observed during the calibration nights (see Table 1) were assumed to have average apparent magnitudes equal to those reported in the Véron-Cetty & Véron (1993) catalog. The photometric errors achieved in our survey are relatively low (the median value of δ_ϵ is 0.019), what allows the detection of low levels of variability.

All the observations made within 5 days were grouped in a single observation- an epoch. The entry n_e in Table 1 refers to these grouped observations. The median number of epochs per quasar is 8, and the median time interval covered by the observations is 2.7 and 1.7 years, in the observer and quasar rest-frame, respectively. Table 2 summarizes some features of the sample, presenting the median values of most of the entries in Table 1, for all objects of the sample as well as for the radio-loud and radio-quiet sub-samples.

Table 2. Median values of some quantities of the sample

	all sample	radio-loud	radio-quiet
number	50	35	15
z	0.544	.614	.385
V	16.17	16.26	16.06
M_V	-26.42	-26.64	-25.36
n_e	8	8	9
Δt_{obs} (yr)	2.74	2.74	2.82
Δt_{rest} (yr)	1.74	1.73	1.74
δ_{obs}	.079	.106	.057
δ_ϵ	.019	.019	.016

2.3 Light Curves

The differential light curves of the quasars in our sample are shown in figures 2 to 8. Each data point ($\Delta V \equiv$ quasar magnitude minus reference star magnitude) corresponds to the average of all the observations collected in each epoch, and the error bars are the corresponding photometric errors.

The observed light curves present a rich variety of forms. Some objects show a monotonical increase or decrease in luminosity (e.g. 3C 273, PKS 2128-12, 4C 09.72), while others seem to exhibit a pulse-like pattern (PKS 1912-549). However, the time-scale covered by the observations (and also the sampling rate) is not large enough to allow an appropriate discussion of the form of the light curves. Since we continue monitoring this sample, we postpone this discussion for a future paper, where we will discuss the data collected over a larger time interval.

3 MEASUREMENTS OF VARIABILITY

3.1 Variability Index

The variability analysis in this paper will be done in terms of luminosity, instead of magnitudes. This procedure makes the comparison with model predictions more direct. We estimate the variability of a quasar with a “robust” index similar to that used by Hook et al. (1994):

$$\sigma_{obs} = \frac{1}{n_e - 1} \sqrt{\frac{\pi}{2}} \sum_{i=1}^{n_e} |L_i - L| \quad (1)$$

where n_e is the number of epochs, L_i is the quasar luminosity in the V band at the i -th epoch, and L is the mean quasar luminosity. The factor $\sqrt{\pi/2}$ assures that for a Gaussian distribution of observations $\{L_i\}$, this index is also an estimator of the standard deviation of the distribution. Several other estimators of variability could be used (e.g., the ordinary standard deviation or the light-curve amplitude), but the results described below are, to a large extent, independent of the variability index employed in the analysis.

The observed variability depends not only of the quasar variability, but also of the observational errors, and the estimation of the *intrinsic* variability σ requires some hypothesis on the distribution of $\{L_i\}$ and their observational errors. If we assume them both Gaussian distributed, the observed and intrinsic variabilities are related by

$$\sigma_{obs}^2 = \sigma^2 + \epsilon^2 \quad (2)$$

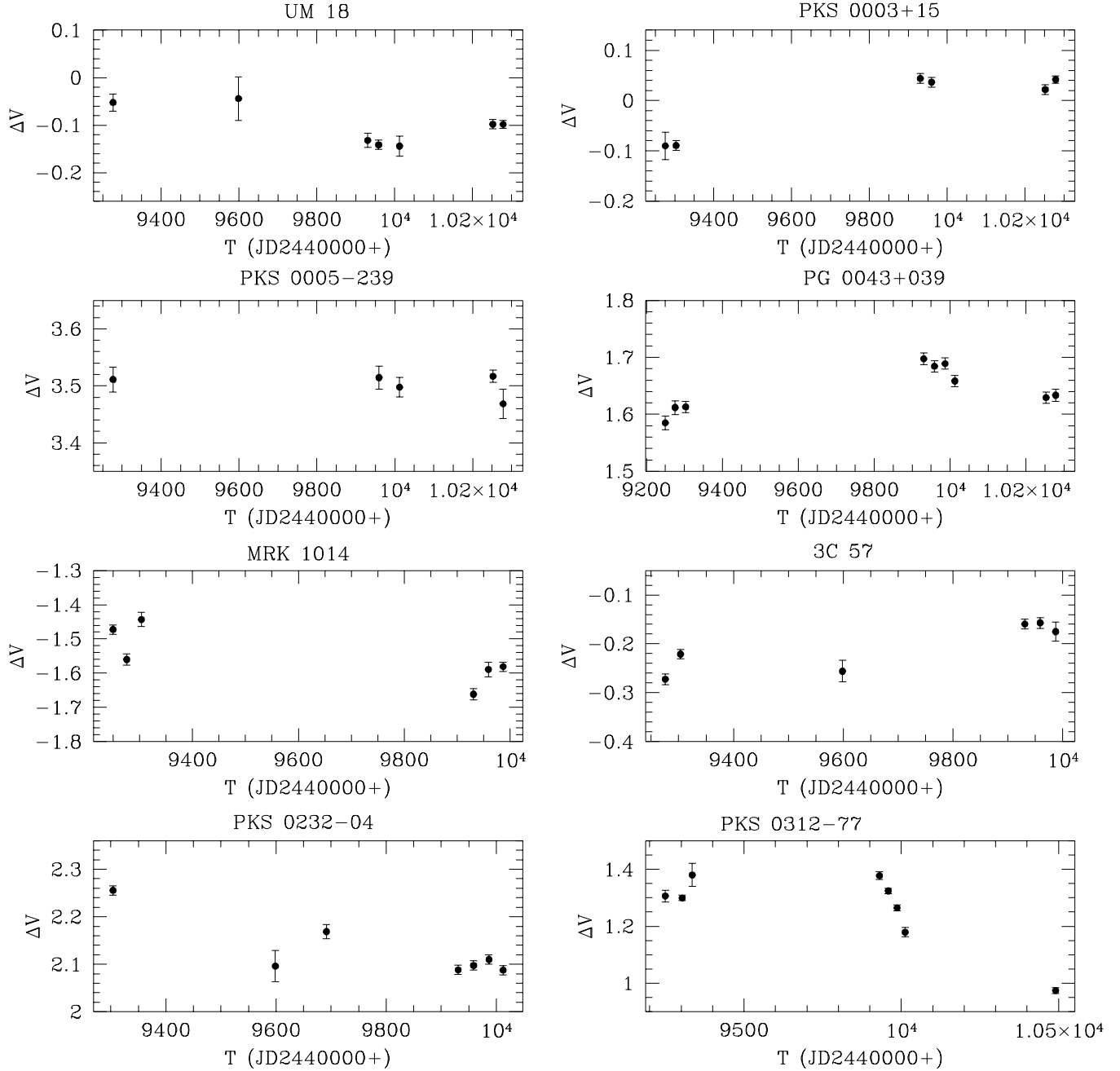


Figure 2. Differential light curves of the sample. ΔV is the difference between the magnitudes of the quasar and the corresponding reference star.

where ϵ^2 is the mean square photometric error in luminosities.

Sometimes it is more useful to work with relative variability, $\delta = \sigma/L$, than with σ or σ_{obs} directly. Note that δ is directly related to the variability measured in magnitudes, $\sigma_m \simeq 0.921 \sigma/L$. The relative photometric error is $\delta_\epsilon = \epsilon/L$.

We will hereafter designate the observed relative variability by δ_{obs} . In figure 9 we display δ_{obs} as a function of absolute magnitude and redshift. It is also shown the median variability values and the corresponding quartiles within bins with equal number of quasars (10). The two objects with largest

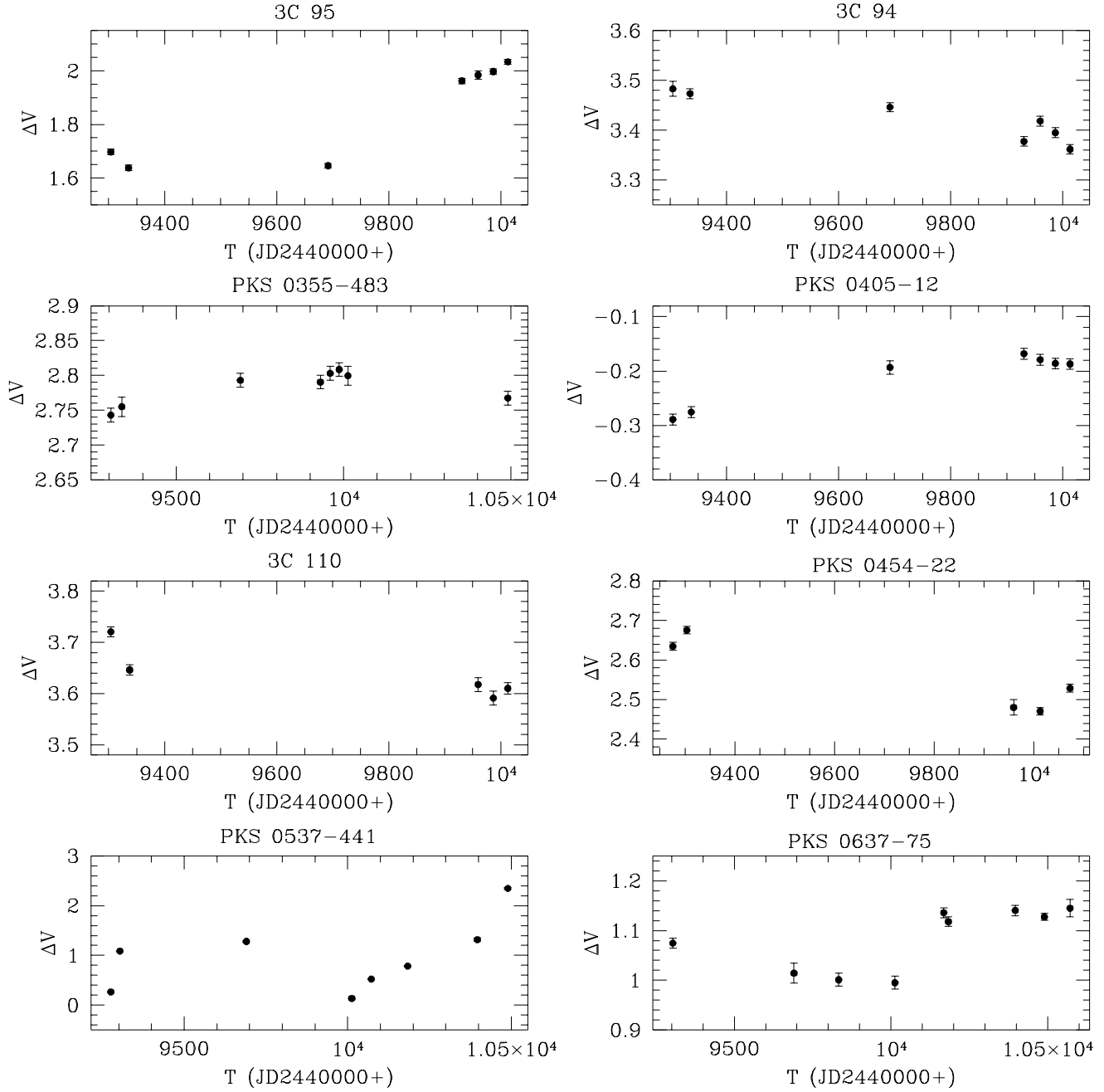


Figure 3. Differential light curves of the sample - cont.

variability in figure 9 are the high polarization quasars PKS 0537-441 and PKS 0736+01.

The data shown in figure 9 are consistent with a decrease of the observed variability with both luminosity and redshift. In fact, the Spearman rank-order correlation coefficient is 0.37 and -0.35, for the $\delta_{obs} \times M_V$ and $\delta_{obs} \times z$,

respectively. The corresponding probabilities for the null hypothesis of uncorrelated data sets is small, 7.7×10^{-3} and 1.4×10^{-2} , respectively, indicating that these trends are statistically significant. Note that the strong correlation between M_V and z present in our sample (figure 1-d) preclude

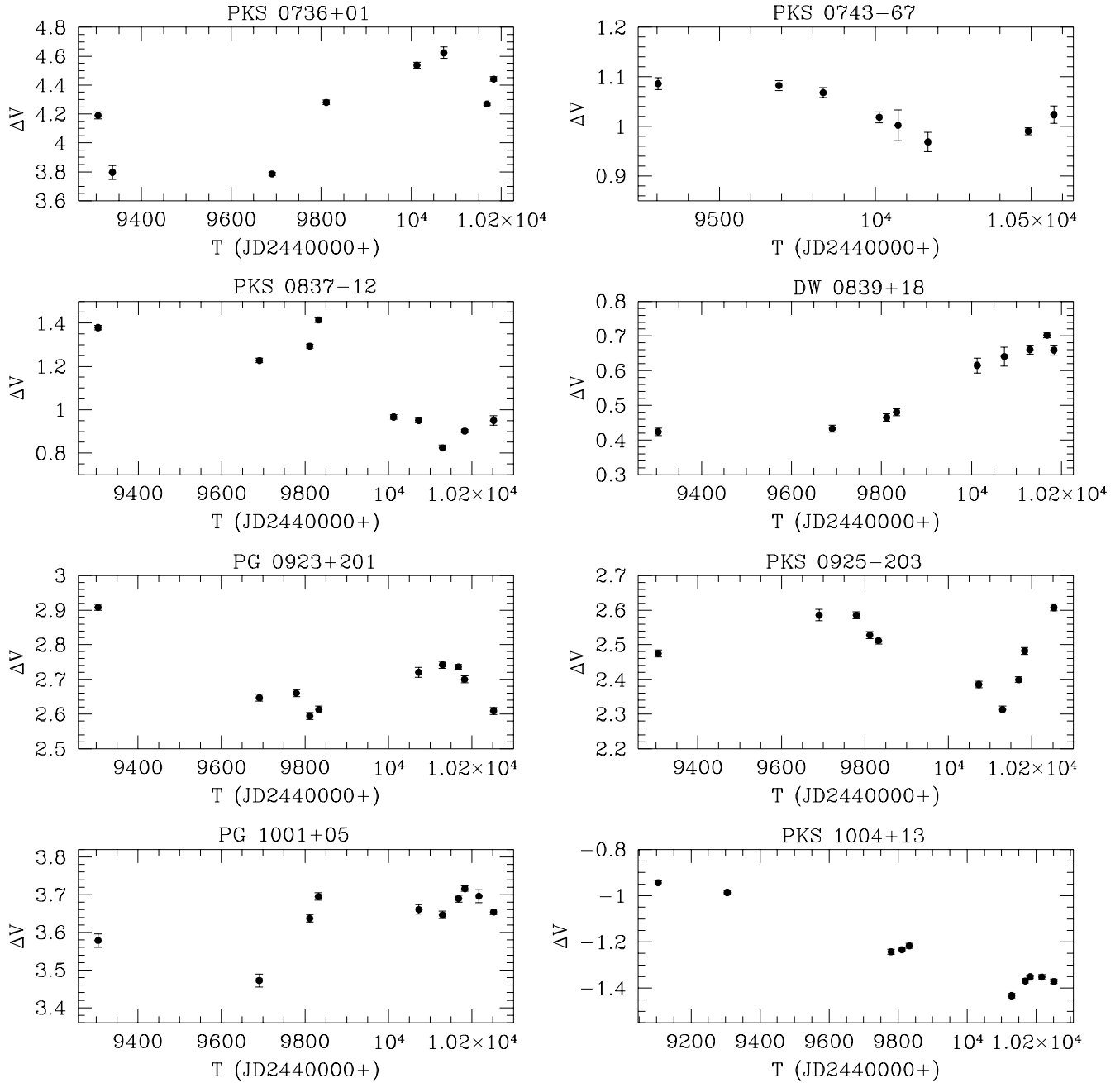


Figure 4. Differential light curves of the sample - cont.

us of knowing what is the real dependence of the variability with respect to both M_V and z .

The quasars in our sample span a large range in redshift; consequently our observations sample different parts of their rest-frame spectra. This makes a direct comparison of the variability of objects somewhat meaningless, unless a

correction for the increase of variability with frequency discussed in the introduction is applied. Next section presents a model for such a correction.

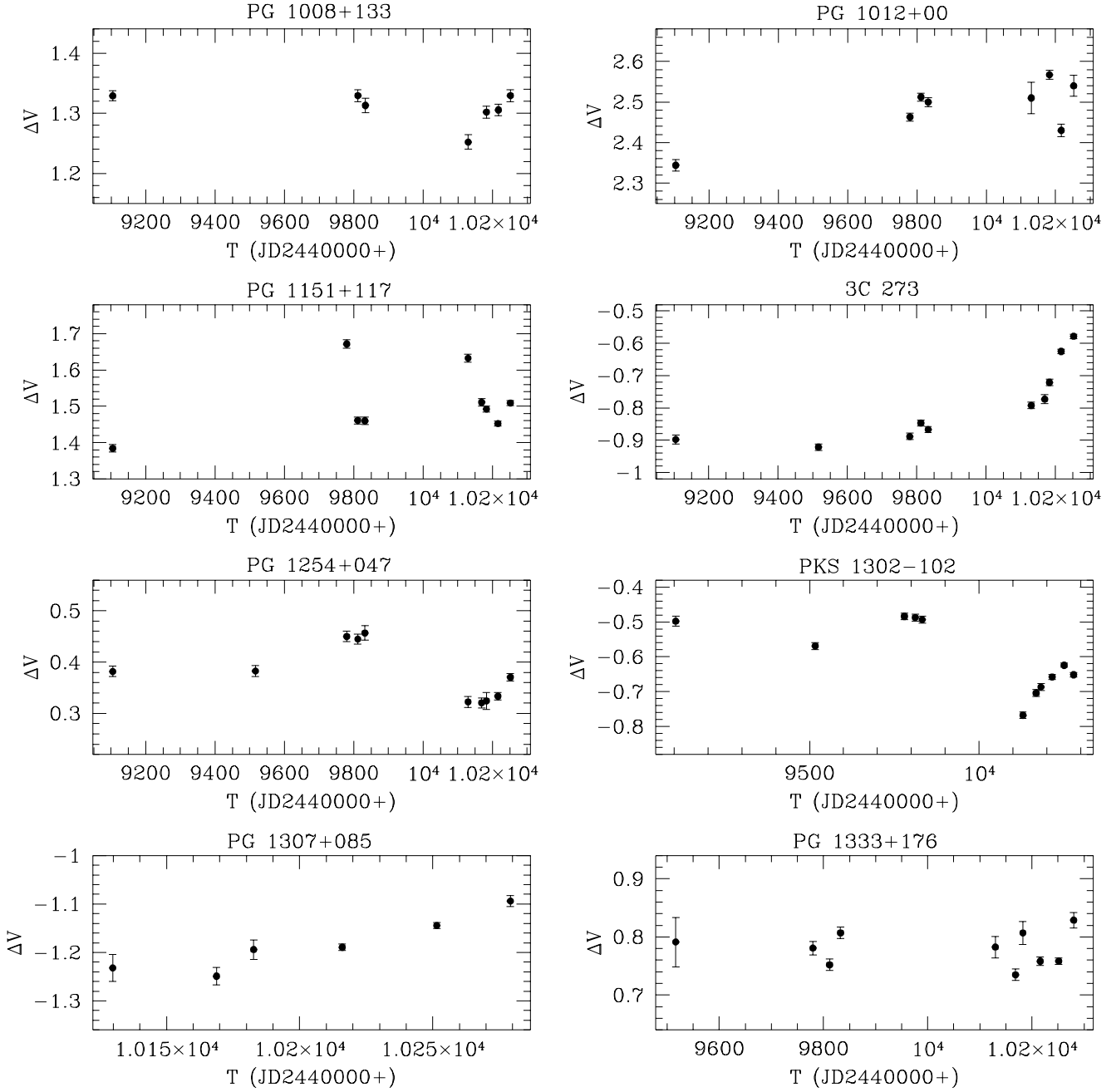
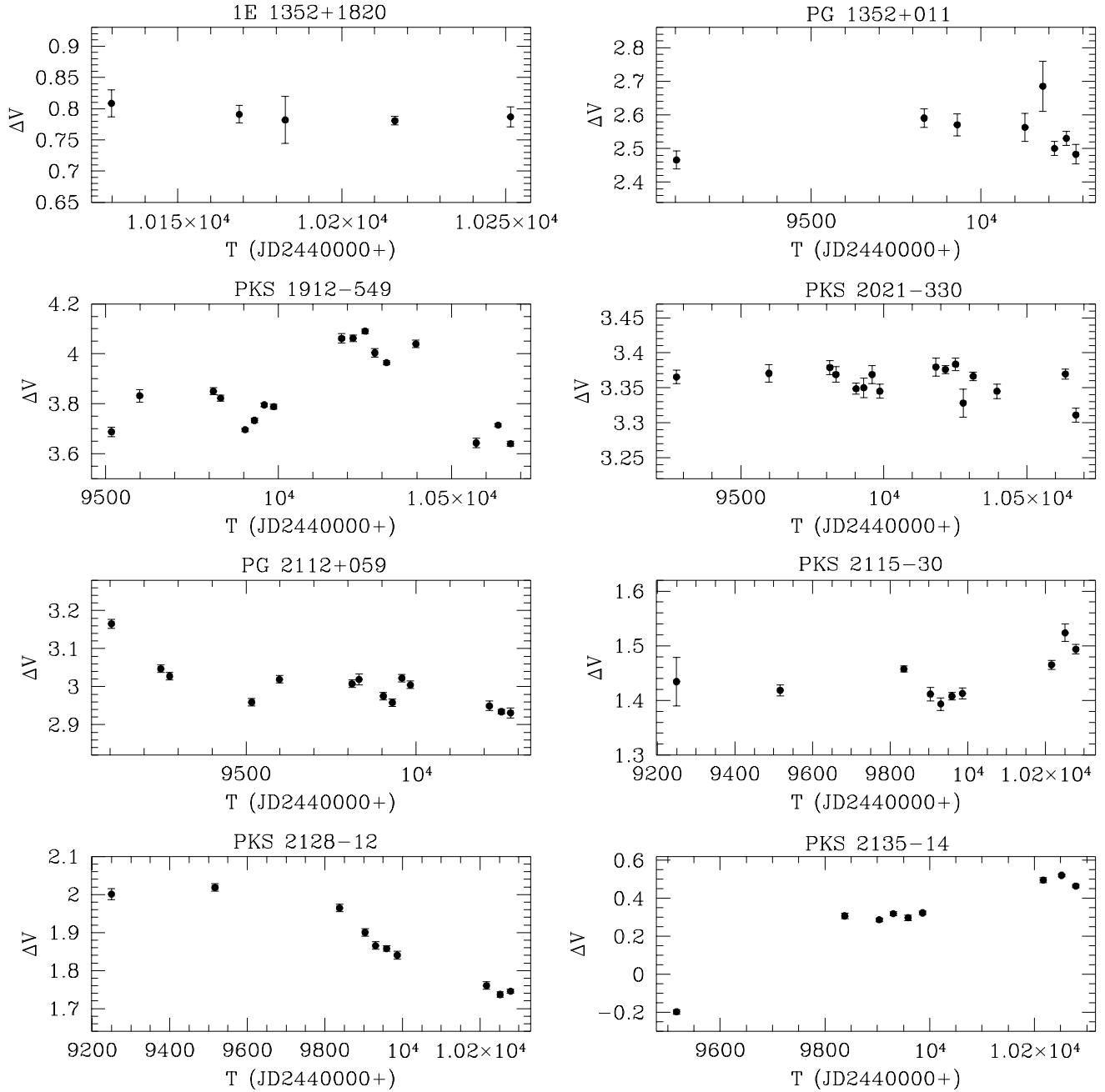


Figure 5. Differential light curves of the sample - cont.

3.2 Variability \times Frequency

Let us suppose that the spectral energy distribution of a quasar in the optical-UV region of the spectrum is a power-law, $f_\nu = f_*(\nu/\nu_*)^\alpha$, where ν is measured in the quasar rest-frame. The increase of the variability with frequency can be interpreted as a hardening of the spectrum associated

to an increase of luminosity. Following Giallongo, Trevese & Vagnetti (1991), we assume that the spectral index increases when the source brightens, keeping the flux unchanged in some near-IR rest-frame frequency ν_* (Cutri et al. 1985). Edelson, Krolik & Pike (1990) have found strong correlations between α_{UV} and the UV flux for the CfA Seyfert 1 galaxies.

**Figure 6.** Differential light curves of the sample - cont.

The same kind of correlation is exhibited by the radio-loud quasar 3C273 (Paltani & Curvoisier 1994). We model these spectral changes as

$$\alpha = \bar{\alpha} + \gamma_0 \log \left(\frac{F_{\nu_0}}{\bar{F}_{\nu_0}} \right) \quad (3)$$

where $\bar{\alpha}$ is the mean spectral index and ν_0 denotes a reference frequency (e.g., a filter) in the observer rest-frame. Despite some observational evidence that $\bar{\alpha}$ may be correlated with the quasar average luminosity, we will assume that it is constant and equal to -0.3, a value appropriate for the optical and UV parts of the spectrum (Francis 1996, Pe-

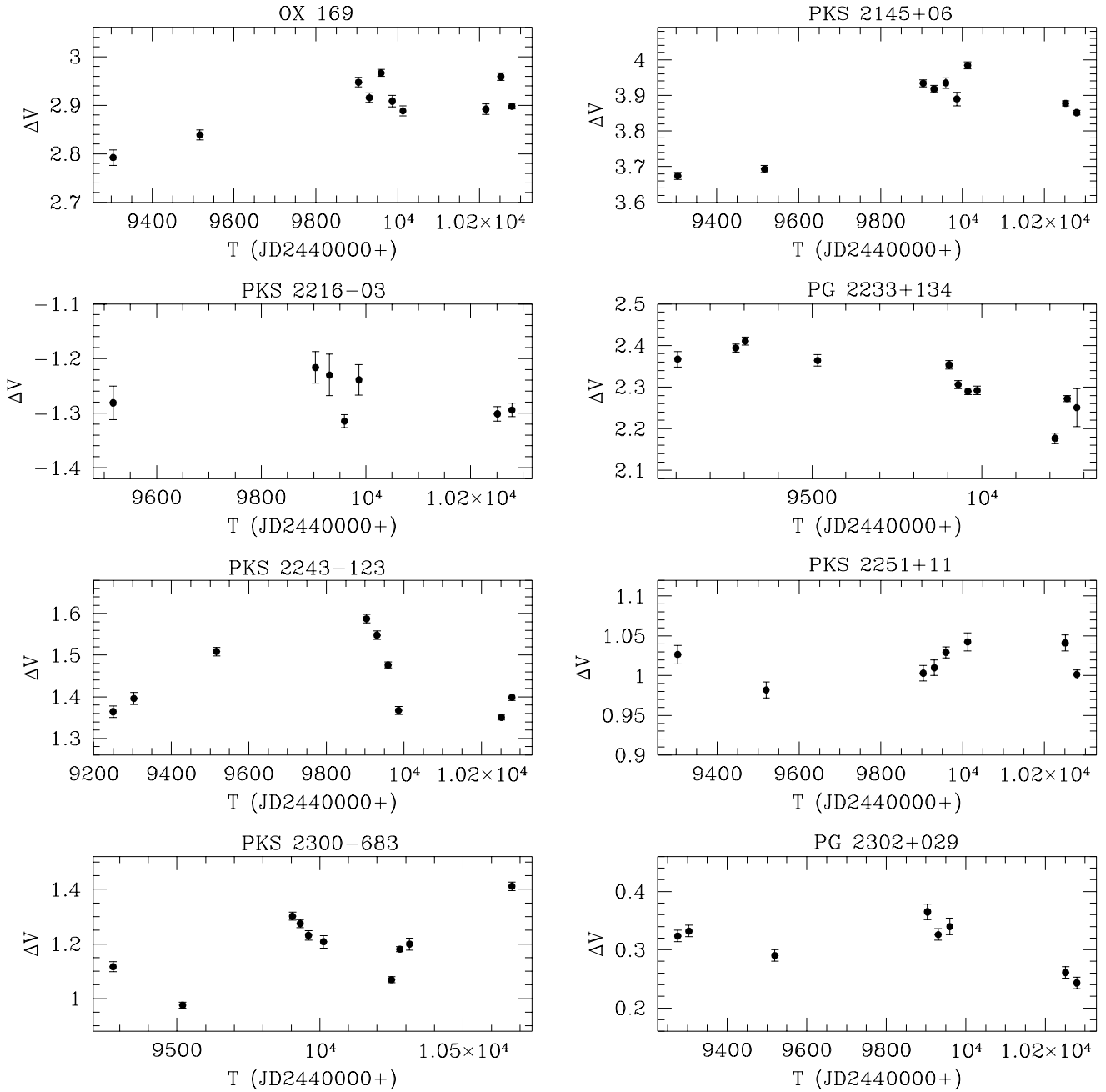


Figure 7. Differential light curves of the sample - cont.

terson 1997). This value is also consistent with that we have adopted for the k -correction (section 2.1). In Eq. (3), \overline{F}_{ν_0} is the average continuum flux integrated in a band centred on ν_0 , i.e., $\overline{F}_{\nu_0} \approx f_{\nu} \Delta\nu$, where $\Delta\nu$ is the filter bandwidth. γ_0 is a parameter that depends only of ν_0 . Note that the rest-frame frequency that is actually measured by a filter with

effective frequency ν_0 is $\nu = (1+z)\nu_0$, where z is the quasar redshift.

From Eq. (3), a small change δF_{ν_0} in the quasar continuum flux produces a change in spectral index given by $\delta\alpha = \gamma_0(\log e)\delta \ln F_{\nu_0}$. Since

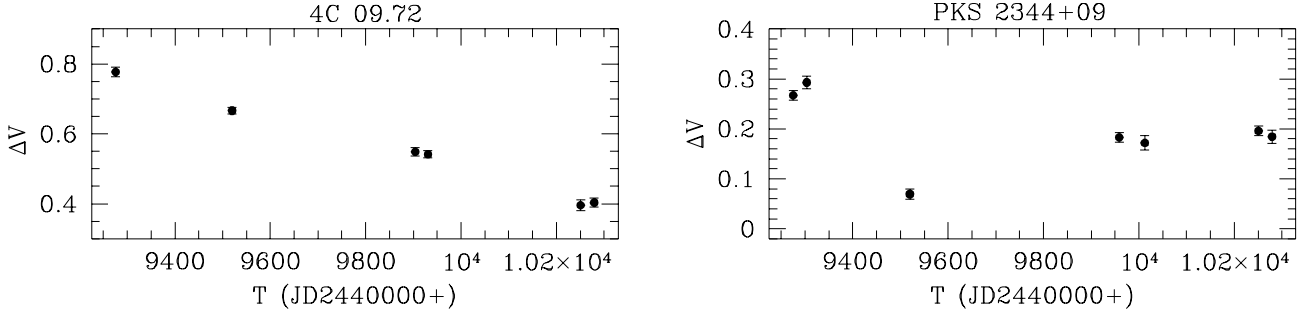


Figure 8. Differential light curves of the sample - cont.

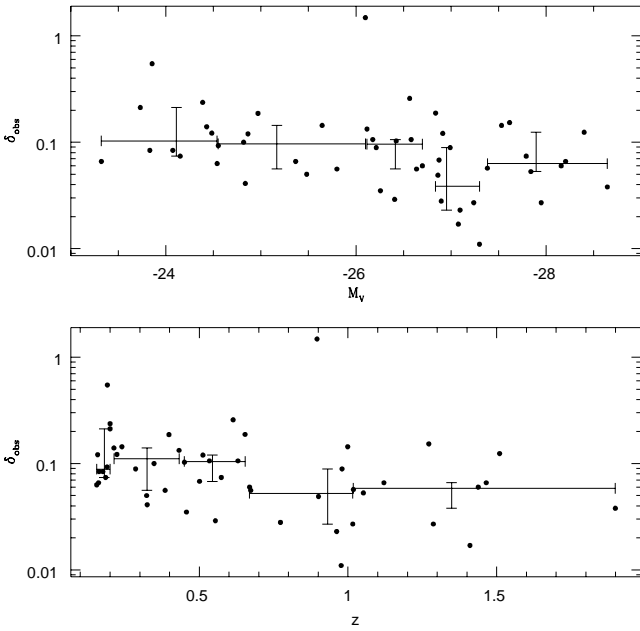


Figure 9. Observed dependences of the variability on luminosity and redshift for our sample. Crosses represent the median values over bins of equal number of objects (10). The vertical bars correspond to the quartiles of the observed variability inside the bins, and the horizontal bars give the range in luminosity of the objects in each bin.

$$\delta \ln f_\nu = \ln \left(\frac{\nu}{\nu_*} \right) \delta \alpha, \quad (4)$$

we have that the monochromatic continuum flux of a quasar varies with frequency as

$$\frac{\delta f_\nu}{f_\nu} = \gamma_0 \log \left(\frac{\nu}{\nu_*} \right) \frac{\delta F_{\nu_0}}{F_{\nu_0}} \quad (5)$$

Let us now consider the relative variability of the flux F_{ν_1} , measured within a band centred on a certain frequency ν_1 , as

$$\delta_{\nu_1} \equiv \frac{\delta F_{\nu_1}}{F_{\nu_1}} \simeq \frac{\delta f_\nu}{f_\nu} \quad (6)$$

where, now, $\nu = (1+z)\nu_1$ is the rest-frame frequency. Note that in the above formula we did not take into account the line-emission correction used before to compute the absolute magnitudes of the quasars. In fact, for objects with redshifts lower than 2.0 (our case) this correction implies differences of at most $\sim 12\%$ in δ_V (i.e., δ measured in the V band), so we decided to neglect such effect. Then, it is easy to verify that the relative variability of a quasar measured in two filters with effective frequencies ν_1 and ν_2 are related as

$$\frac{\delta_{\nu_1}}{\delta_{\nu_2}} = \frac{\log((1+z)\nu_1/\nu_*)}{\log((1+z)\nu_2/\nu_*)} \quad (7)$$

We have estimated $\lambda_* = c/\nu_* \approx 11400\text{\AA}$ from data of Edelson, Krolik & Pike (1990), by fitting Eq. (7) for $\lambda_1=1450\text{\AA}$ and $\lambda_2=2885\text{\AA}$; we have used all objects studied by those authors with the exception of NGC 7469, that seems to present a different variability pattern. Using data for 3C273 from Paltani & Curvoisier (1994), we obtain a similar value, $\lambda_* \approx 11250\text{\AA}$.

This very simple model for the frequency dependence of variability is indeed able to explain the variability behaviour of the nucleus of the Seyfert galaxy NGC 4151. For this exercise, we have used data collected in several spectral bands by Edelson et al. (1996). Firstly, we removed from the observed fluxes the light contribution of the host galaxy, accordingly to the recipe given in the paper. After, we fitted Eq. (7) to the relative variability as a function of the frequency, obtaining $\lambda_* \approx 8400\text{\AA}$ for data in the optical and UV. The fit of the model to the data is very good, as shown in figure 10, and has a linear correlation coefficient of -0.92 . Surprisingly, including the data point corresponding to the intermediate X-ray emission (1.5 keV), the correlation becomes even stronger ($r=-0.99$) and λ_* increases to $\sim 9500\text{\AA}$. This last result, however, may be somewhat fortuitous because we did not take into account any correction for the X-ray absorption. Anyway, our variability model seems to fit very well the overall variability pattern observed in NGC 4151. In what follows, we adopt $\lambda_* = 1 \mu\text{m}$ as the pivot wavelength, since the results are not strongly dependent on the value of λ_* (see section 4.2). Note that near $1 \mu\text{m}$ there is also a minimum in the spectral energy distribution of quasars, separating the bump that extends towards

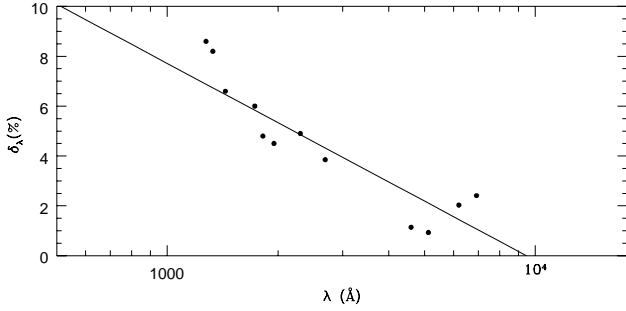


Figure 10. Relative flux variation (in percentage) of the NGC 4151 nucleus (from data of Edelson et al. 1996) as a function of the logarithm of wavelength. The straight line represents a simple (unweighted) linear fit.

the infrared (attributed to thermal emission by dust) from the optical-UV Big Blue Bump.

Let δ_{obs} be the relative variability observed in the V band and δ_{rest} the relative variability that we would observe in the V band if the quasar was at $z = 0$. Since the V band in the observer frame corresponds to a frequency $(1+z)\nu_V$ in the rest-frame of a quasar at redshift z (where ν_V is the V band characteristic frequency), we have that

$$\frac{\delta_{rest}}{\delta_{obs}} = \frac{\log(\nu_V/\nu_*)}{\log((1+z)\nu_V/\nu_*)} \quad (8)$$

Note that the relative variability is independent of the k -correction.

These expressions can be used to transform the observed variability of the quasars of our sample to rest-frame variability. For instance, Eq.(8) can be rewritten numerically as

$$\delta_{rest}^2 = \left[\frac{0.260}{\log(1.818(1+z))} \right]^2 \times (\delta_{obs}^2 - \delta_e^2) \quad (9)$$

where we have included the effect of observational errors in quadrature, accordingly to Eq. (2).

The effect of the correction is to reduce the observed variability. For the most distant object in our sample ($z=1.899$) this reduction is 36%.

The application of this correction decreases slightly the scattering in the relations between relative variability and absolute magnitude or redshift. The Spearman correlation coefficients (r_S) calculated with data corrected by the measurement errors and frequency dependence are 0.38, for $\delta_{rest}^2 \times M_V$, and -0.36, for $\delta_{rest}^2 \times z$, to be compared with the values before the frequency dependence correction, 0.25 and -0.22, respectively.

4 IS THE VARIABILITY POISSONIAN?

4.1 A Simple Poissonian Model

The non-periodicity of pulses in the light curves of quasars and Seyfert galaxies, as well as the observed anti-correlation

between their variability and luminosity can be viewed as an evidence favouring the sub-units model. In the Starburst model (Terlevich et al. 1992), for example, the variability is produced by supernova explosions and the interaction of their ejecta with a high-density circumstellar medium. The superposition of random individual pulses would be responsible by the Poissonian character of this model. Even not being traditionally faced this way, the accretion disc model itself could accommodate a Poissonian behaviour, as long as the instabilities that would cause the variability act as independent events (Cid Fernandes, Aretxaga & Terlevich 1996). The same may be expected in models where the variability is produced by external effects, if these too are independent of each other.

Let us consider here the Poissonian model in its simplest version (e.g., Paltani & Courvoisier 1997 or Cid Fernandes 1995). The light curve of a quasar is described as a superposition of random pulses over a component of constant luminosity L_c , and depends only on three parameters related to the pulses: their rate (n), energy (E), and effective time-scale (t_p). If $l(t)$ is the typical luminosity profile of a pulse, we may define

$$E \equiv \int l(t) dt \quad (10)$$

and

$$t_p \equiv \frac{[\int l(t) dt]^2}{\int l(t)^2 dt} \quad (11)$$

Then, it can be shown that the average luminosity of a quasar is

$$L = L_c + L_{var} = L_c + nE \quad (12)$$

and that its variance is given by

$$\sigma^2 = \frac{E^2 n}{t_p} = \frac{EL_{var}}{t_p}, \quad (13)$$

where L_{var} is the variable component of the luminosity.

Let f_{var} be the fraction of the average luminosity due to the variable component: $f_{var} = L_{var}/L$. Then, the variance of the quasar luminosity can be written as

$$\sigma^2 = \frac{E^2 n}{t_p} = \frac{E f_{var} L}{t_p}, \quad (14)$$

and the relative variability is

$$\delta = \frac{\sigma}{L} = \left(\frac{f_{var} E}{L t_p} \right)^{1/2} \quad (15)$$

Therefore, if f_{var} , E and t_p are independent of the luminosity, σ and δ must be proportional to $L^{1/2}$ and $L^{-1/2}$, respectively. We will call this scenario as the simple Poissonian model. In this model, quasars differ from each other only by their rate of events, n .

4.2 Testing the Poissonian Hypothesis

As mentioned before, due to the strong correlation present in the luminosity vs. redshift diagram, we are unable to obtain with our sample the joint dependence of the variability

on luminosity and redshift. So, in order to test the simple Poissonian model, we will neglect any dependence of variability on redshift. This assumption is justified by results of some previous variability studies, that have not found any significant dependence of the variability vs. luminosity anti-correlation with redshift (e.g., Hook et al. 1994; Cristiani et al. 1996).

In order to verify whether our data is consistent with the Poissonian scenario, we model the corrected relative variability δ_{rest} as

$$\delta_{rest}^2 = \frac{a}{L^b} \quad (16)$$

where a and b are free parameters. In the simple Poissonian model the expected value of b is 1. We will work with δ_{rest}^2 instead of δ_{rest} because for some objects the observed variability is smaller than the observational errors, leading to negative values in the right side of Eq.(9). Our approach avoids discarding these data points.

The parameters a and b were obtained with a ‘‘robust’’ version of χ^2 . Let us define the residual u_i of the variability of the i -th quasar, weighted by its relative observational error, as

$$u_i = \frac{(\delta_{rest,i}^2 - a/L_i^b)}{\delta_{\epsilon,i}^2} \quad (17)$$

In traditional χ^2 , the parameters a and b may be determined by minimizing the mean value of the set $\{u_i^2\}$. Here we estimate these parameters by minimizing the median of $\{|u_i|\}$. This approach is less sensitive to the variability behaviour of objects with extreme properties, like the high polarization quasars and the objects with very low variability. The uncertainties in the parameters were obtained by bootstrap re-sampling of the observed data sets (Feigelson & Babu 1992).

The results of the application of this method to our data are shown in Table 3. We have obtained $a = 0.05 \pm 0.25$ and $b = 1.20 \pm 0.58$ (for L_V in units of $10^{10} L_\odot$). The large values of the errors reflect the large spread of quasar variability at a given luminosity, as can be seen in figure 9 or in figure 11, where we plot δ_{rest} as a function of the luminosity of the objects, both in linear and logarithmic scales. The continuous line represents the best fit for all the sample. From the bottom plot in figure 11, it can be seen that excluding from the analysis objects for which δ_{rest}^2 is negative would lead to a shallower slope ($b = 0.69 \pm 0.36$ instead of $b = 1.20 \pm 0.58$) for the variability versus luminosity relationship.

A very interesting result is that the best-fit value of b is always very near the value $b = 1$ expected in the simple Poissonian model. As shown in Table 3, even for the radio-quiet and radio-loud sub-samples we have obtained values of b consistent, within the errors, with the simple Poissonian model. The dashed line in figure 11 represents the best-fit solution for the simple Poissonian model. It is worth noting that the a and b values obtained from this analysis are rather insensitive to changes in the pivot wavelength λ_* . For instance, modifying λ_* by 1000 \AA leads to changes much less than 1σ in the best-fit values of a and b .

If we assume that the quasar variability may indeed

be described by the simple Poissonian model, then the only free parameter now, a , can be estimated by minimizing the median of $\{|u_i|\}$ with $b = 1$. These results are also shown in Table 3. In this case the parameter a can be used to constrain the energy of the individual pulses, E , because

$$E = \frac{a \times t_p}{f_{var}} \quad (18)$$

Assuming that f_{var} is in the range 0.5-1.0 (Cid Fernandes, Aretxaga & Terlevich 1996 adopted a lower limit of 0.3), and a typical pulse time-scale t_p of 1.5 to 3.0 years (see, for example, the structure function analysis of Hook et al. 1994, and the discussion in Cid Fernandes, Aretxaga & Terlevich 1996), we get individual energy pulses falling in to the interval $2.5 \times 10^{49} - 1.5 \times 10^{50}$ erg in the rest-frame V band. We can compare these results with those obtained in the analysis of Cid Fernandes, Aretxaga & Terlevich (1996). For quasars, we may assume that $L_V \sim 0.66 \times L_B$ (for $\alpha = -0.3$). Then, the energy range found by those authors is $1.0 \times 10^{50} \lesssim E \lesssim 4.1 \times 10^{51}$ erg in the V band. This energy interval is not inconsistent with our results. A recent study of the bright quasar 3C273 by Paltani, Courvoisier & Walter (1998) indicates that its pulse energy in the optical-ultraviolet spectral range is $\sim 3 \times 10^{51}$ erg. The corresponding energy in the V band is about one order of magnitude smaller, that is also consistent with our results.

Table 3. Parameters obtained from the robust fits, for all data and for the radio class sub-samples. We present results assuming $b = 1$ (simple Poissonian model), as well as for the case where a and b are free parameters. The symbol # refers to the number of data points used in the fit. The parameters were calculated with V luminosities in units of $10^{10} L_{\odot}$.

	a	b	number
All Sample	0.050 ± 0.254	1.20 ± 0.58	50
	0.030 ± 0.017	1	50
Radio-Loud	0.130 ± 0.395	1.43 ± 0.50	35
	0.040 ± 0.054	1	35
Radio-Quiet	0.020 ± 0.150	1.22 ± 0.81	15
	0.014 ± 0.010	1	15

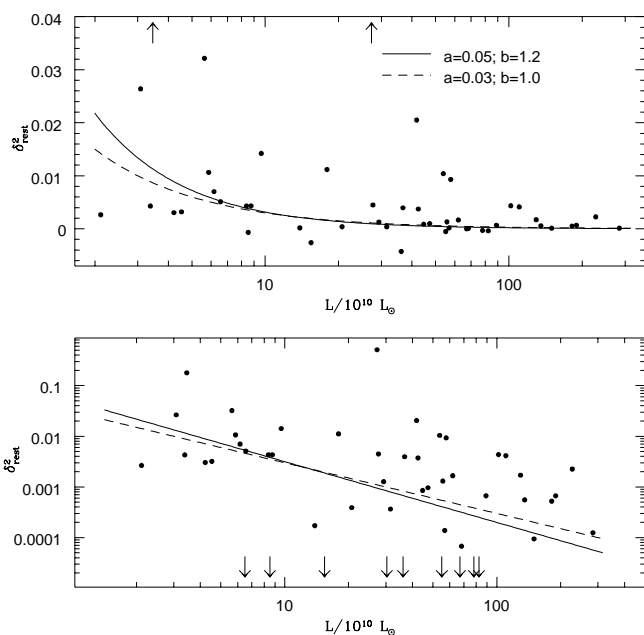


Figure 11. Rest-frame variability as a function of luminosity for our sample. The continuous line represents the best-fit result assuming a and b as free parameters, whereas the dashed line is the best-fit for the simple Poissonian model ($b = 1$). The fittings correspond to the “all sample” parameters in table 3.

5 VARIABILITY OF RADIO-LOUD AND RADIO-QUIET QUASARS

Radio-loud and radio-quiet quasars (hereafter in this section RL and RQ, respectively) present almost the same continuum spectral characteristics, with the exception of their radio emission, where they differ by about 3 orders of magnitude. It has been observed a trend for RL be more variable than RQ (Pica & Smith 1983), what can be due to a contribution of the collimated components associated to the non-thermal emission (Netzer et al. 1996). Some studies have suggested the existence of an intermediate class, where the small scale jets observed in some RQ would be directed

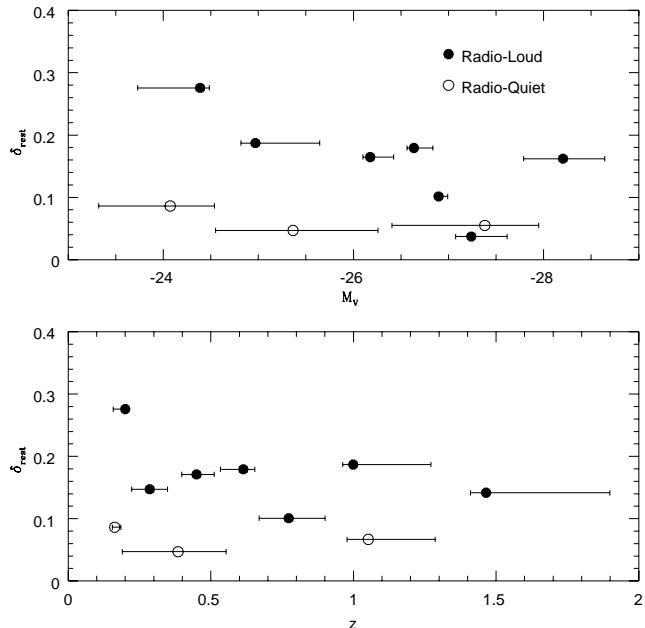


Figure 12. Median rest-frame variability as a function of absolute magnitude and redshift for radio-loud (filled circles) and radio-quiet (open circles) quasars. The horizontal lines give the interval of M_V or z corresponding to each bin.

along the line-of-sight (Miller, Rawlings & Saunders 1993; Kellermann et al. 1994; Blundell & Beasley 1998).

The median values for the variability of RL and RQ, corrected for the variability-frequency effect are, respectively, δ_{rest} equal to 0.063 and 0.019. Consequently, for our sample, the rest-frame relative variability of RL is about 3 times larger than for RQ. About the same factor is found for the parameter a in the simple Poissonian model, as shown in Table 3. However, RL in our sample tend to be more luminous and have higher redshift than RQ: the median M_V is -26.6 and -25.4 for RL and RQ, respectively, and the corresponding median redshifts are 0.61 and 0.39. According to our previous discussion, the relative variability decreases with increasing luminosity, and, given the differences of the median values of the luminosities of the objects in these two classes, the real difference in the corrected relative variability of RL and RQ should be even larger. Actually, RL tend to be more variable than RQ over all magnitudes and redshifts, as can be seen in figure 12, where we plot median variability values calculated in bins with equal number of objects. Our observations then confirm earlier results obtained by Pica & Smith (1983).

6 SUMMARY AND CONCLUSIONS

In this paper we have presented the first results of a photometric monitoring of quasars that have been conducted at CNPq/Laboratório Nacional de Astrofísica, in Brazil, since 1993. The observations discussed here were done in the V

band and span the period between March 1993 and July 1996. This set of observations has good photometric accuracy ($\sim 0.019 V$ mag), achieved through differential photometry with CCD detectors, what allows the detection of low levels of variability.

The relative variability observed in the V band, δ_{obs} , decreases with increasing luminosity and redshift. However, our observations in the V band sample different rest-frame frequencies for quasars at different redshifts, and it is convenient to convert all observations to a single rest-frame frequency (e.g., that of the V band) in order to compare the variability properties of these objects. In computing δ_{rest} , the relative variability expected in the rest-frame V band of the quasars, we have taken into account a model for the increase of the variability with frequency, assuming that an increase in luminosity corresponds to a hardening of the spectrum. This model turned out to be consistent with the nuclear variability observed during multi-wavelength observations of the Seyfert galaxy NGC 4151 (Edelson et al. 1996).

We have noticed that correcting the relative variability by applying the model above decreases the scatter in the anti-correlation of δ with z or L , increasing slightly the significance of the relations between these quantities. Such anti-correlations are in agreement with results of other studies, like Hook et al. (1994) and Cristiani et al. (1996). Note that the strong correlation in the $M_V \times z$ diagram for the objects in our sample preclude us of disentangling the real dependences of the variability on these two parameters.

We have verified that the relative variability δ_{rest} tends to decrease with the luminosity in agreement with the expectations of a simple Poissonian model, where the light curves are assumed to be the result of a random superposition of pulses of same energy. Characteristic energies for individual pulses derived with such a model are consistent with those predicted by the nuclear starburst scenario (e.g., Cid Fernandes, Aretxaga & Terlevich 1996). Assuming that there are no differences in n , f_{var} and t_p for both classes, the pulse energies for the radio-loud objects are larger than for radio-quiet objects by almost one order of magnitude. The radio-loud objects in our sample tend to be more variable than radio-quiet objects.

ACKNOWLEDGEMENTS

This work benefited from the financial support provided by the Brazilian agencies FAPESP and CNPq. We are grateful to Eduardo Cypriano and Héctor Cuevas for helping in the observations, and to Roberto Cid Fernandes and Sueli Viegas for fruitful discussions.

REFERENCES

Allen C.W., *Astrophysical Quantities*, 3th Edition, 1976
 Aretxaga I., Cid Fernandes R., Terlevich R.J., 1997, MNRAS, 286, 271
 Bessel M.S., 1990, PASP, 102, 1181
 Borgeest U., Schramm K.J., 1994, A&A, 284, 764
 Blundell K.M., Beasley A.J., 1998, MNRAS, to be published

Cid Fernandes R., 1995, PhD thesis, Cambridge, England
 Cid Fernandes R., Aretxaga I., Terlevich R., 1996, MNRAS, 282, 1191
 Cimatti A., Zamorani G., Marano B., 1993, MNRAS, 263, 236
 Cristiani S., Trentini S., La Franca F., Andreani P., Aretxaga I., 1996, A&A, 306, 395
 Cristiani S., Trentini S., La Franca F., Andreani P., 1997, A&A, 321, 123
 Cristiani S., Vio R., Andreani P., 1990, AJ, 100, 56
 Cutri R.C., Wisniewski W.Z., Rieke G.H., Lebofsky M.J., 1985, ApJ, 296, 423
 Edelson R., Krolik J., Pike G., 1990, ApJ, 359, 86
 Edelson et al., 1996, ApJ, 470, 364
 Feigelson E.D., Babu G.J., 1992, ApJ, 397, 55
 Francis P., 1996, PASA, 13, 212
 Giallongo E., Trevese D., Vagnetti F., 1991, ApJ, 377, 345
 Giveon U., Maoz D., Kaspi S., Netzer H., Smith P.S., 1999, astro-ph/9902254
 Gopal-Krishna, Sagar R., Wiita P.J., 1995, MNRAS, 274, 701
 Graham J.A., 1982, PASP, 94, 244
 Hook I.M., MacMahon M.G., Boyle B.J., Irwin M.J., 1994, MNRAS, 268, 305
 Kellermann, K.I., Sramek R.A., Schmidt M., Green R.F., Shaffer D.B., 1994, AJ, 108, 4
 Kinney A.L., Bohlin R.C., Blades J.C., York D.G., 1991, ApJS, 75, 645
 Lloyd C., 1984, MNRAS, 209, 697
 Miller P., Rawlings S., Saunders R., 1993, MNRAS, 263, 425
 Netzer H., Heller A., Loinger F., Alexander T., Baldwin J.A., Wills B.J., Han M., Frueh M., Higdon J.L., 1996, MNRAS, 279, 429
 Paltani S., Courvoisier T.J.-L., 1994, A&A, 291, 74
 Paltani S., Courvoisier T.J.-L., 1997, A&A, 323, 717
 Paltani S., Courvoisier T.J.-L., Walter R., 1998, A&A, 340, 47
 Pica A.J., Smith A.G., 1983, ApJ, 272, 11
 Peterson B.M., 1997, *An Introduction to Active Galactic Nuclei*, Cambridge University Press
 Rees M.J., 1984, ARA & A, 22, 471
 Terlevich R., Tenorio-Tagle G., Franco J., Melnick J., 1992, MNRAS, 255, 713
 Trevese D., Kron R. G., Majewski S.R., Bershadsky M.A. & Koo D.C., 1994, ApJ, 433, 494
 Uomoto A.K., Wills B.J., Wills D., 1976, AJ, 81, 905
 Véron-Cetty M.P., Véron P., 1987, ESO Scientific Report, 3rd edition
 Véron-Cetty M.P., Véron P., 1993, ESO Scientific Report, 6th edition